Thermo acoustic study of carbon nanotubes in near and far field: Theory, simulation, and experiment

S. S. Asadzadeh, A. Moosavi, C. Huynh, and O. Saleki

Citation: Journal of Applied Physics **117**, 095101 (2015); doi: 10.1063/1.4914049
View online: http://dx.doi.org/10.1063/1.4914049
View Table of Contents: http://scitation.aip.org/content/aip/journal/jap/117/9?ver=pdfcov
Published by the AIP Publishing

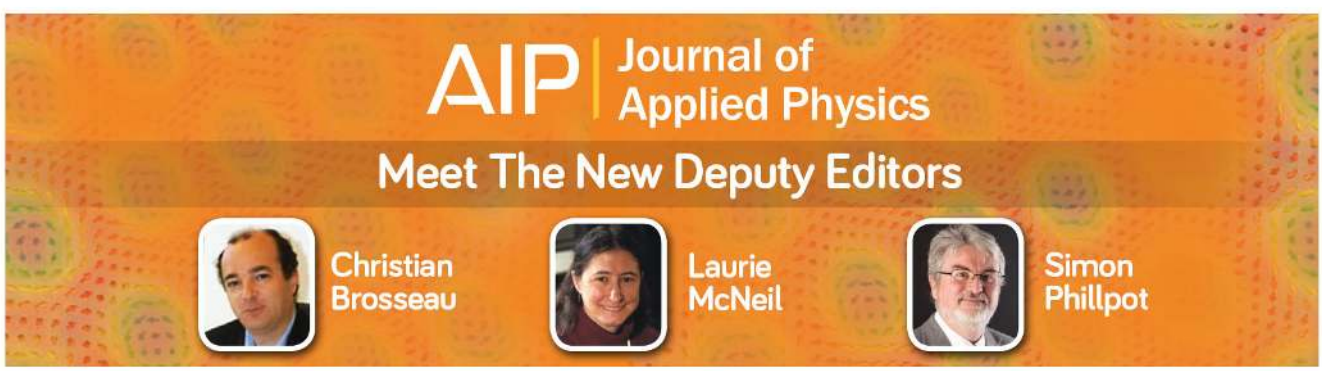

JOURNAL OF APPLIED PHYSICS **117**, 095101 (2015)

Thermo acoustic study of carbon nanotubes in near and far field: Theory, simulation, and experiment

S. S. Asadzadeh,[1] A. Moosavi,[1,a)] C. Huynh,[2] and O. Saleki[1]
[1]*Center of Excellence in Energy Conversion (CEEC), School of Mechanical Engineering, Sharif University of Technology, Azadi Avenue, P. O. Box 11365-9567, Tehran, Iran*
[2]*CSIRO Materials Science and Engineering, Bayview Ave, Clayton Vic 3168, Australia*

(Received 9 December 2014; accepted 22 February 2015; published online 6 March 2015)

Carbon nanotube webs exhibit interesting properties when used as thermo-acoustic projectors. This work studies thermo-acoustic effect of these sound sources both in near and far field regions. Based on two alternative forms of the energy equation, we have developed a straightforward formula for calculation of pressure field, which is consistent with experimental data in far field. Also we have solved full 3-D governing equations using numerical methods. Our three-dimensional simulation and experimental data show pressure waves are highly affected by dimensions of sound sources in near field due to interference effects. However, generation of sound waves in far field is independent of projectors area surface. Energy analysis for free standing Thermo-Acoustic (TA) sound sources show that aerogel TA sound sources like CNT based projectors could act more efficiently compared to the other sources in delivering more than 75% of alternative input energy to the medium gas up to a frequency of 1 MHz. © *2015 AIP Publishing LLC*.
[http://dx.doi.org/10.1063/1.4914049]

I. INTRODUCTION

Thermo-acoustic effect for sound generation has been known for near a century. In 1917, Arnold and Crandall[1] examined 700 nm platinum foils and observed as alternative electrical current passes through the foil, a weak sound would be generated. They correctly attributed this phenomenon to the small Heat Capacity Per Unit Area (HCPUA) of Pl foils and their ability to rapidly conduct heat to the medium; and concluded if the HCPUA of sound source is too small, alternative current results in a periodic temperature oscillation in near medium and consequently a periodic pressure wave. Using Super-aligned Carbon Nanotube with ultra small HCPUA,[2] Xiao *et al.*[3] reported that these CNTs are able to produce sound in wideband frequencies and also in underwater, as reported by Aliev *et al.*[4] Thermo acoustic effect has also been observed in other materials with ultra small HCPUA.[5–9] By making different kind of super-aligned CNTs, Suziki *et al.*[10] examined sound generation of CNTs from a structural web morphology viewpoint and reported no change in sound intensity. It has been reported lower heat capacity of medium[11,12] and encapsulating CNTs based source[13] could increase sound intensity of these sources.

Theories developed in the field of thermo acoustic mostly tried to solve coupled temperature and pressure equations for one dimensional planar or spherical on substrate sources[14–16] and arbitrary source taking advantages of point sources.[17] Some have used temperature variations of either sound source or medium in one dimensional domain and then have ascribed the pressure to the temperature variations,[1,3] which requires some assumptions and simplifications.

In the present study, to avoid dealing with difficulty of solving governing equations for the Thermo-Acoustic (TA) source and medium fluid at the same time, sound generation of source is considered as two parts: first, neglecting heat capacity of heat source and based on two alternative forms of energy equation, we derive a straightforward differential equation which, in contrast with other theories, is decoupled from temperature variations and directly relates pressure to the heat delivered to the fluid. Thus, no assumption is needed to relate temperature variation to the pressure variations. Using this equation, a formula is derived for sound generation of small TA projectors as a function of energy received by fluid. Then, applying energy balance and considering temperature distribution in finite TA source and medium fluid, another formula for energy delivered to the fluid as a function of input energy is calculated. This formula takes into account contribution of sound source in conducting heat to the medium fluid. Combining these two formulas, an analytical model is derived for TA sound sources, which could accurately predict sound pressure in far field. In addition, analyzing the portion of energy delivered to the fluid at different frequency shows CNT based sound sources are nearly perfect materials because of their aerogel nature as well as their ultra small HCPUA, for TA sound generation up to 1 MHz frequency domain which could open their usage in ultrasonic devices for industrial and medical applications like non-destructive testing, drug delivery, and eye surgery.

Although reaching an analytical solution for 3-D governing equations are difficult and, to the best of our knowledge, no attempt to solve these equations has been reported, herein, we solved these equations numerically by finite difference method and obtained pressure field in near and far field regions for different sizes of sound sources at different frequencies. Simulation results for different sound projectors

a)Email: moosavi@sharif.edu

show that sound pressure in near field is extremely dependent on the size of TA source and sound frequency. Experimental measurements using CNT sheets are conducted to verify theoretical and simulation results.

The remainder of the research is organized as follows: Section II develops a theory which is applicable for calculation of pressure in far field. In Sec. III, the numerical method is illustrated. Section IV describes experimental setup. Section V presents theoretical, numerical, and experimental results and discusses the findings. This paper ends in Sec. V by proper conclusions.

II. THEORY

Sound generation of a TA source could be considered as two parts:[18] ability of sound source in conducting heat to the medium gas and pressure variation of medium due to this periodic heat. First, we deal with pressure variation as a function of periodic heat delivered to the medium. Because pressure field emitted from an arbitrary source is highly affected by its dimensions, here we consider a point source which its result is applicable for a general source in far field. However, to calculate the ability of sound source in delivering heat to medium, we take into account TA source shape.

In case of small TA projectors, pressure waves generated by TA effect propagate radically away from sound source as depicted in Fig. 1. Energy equation for compressible, unsteady moving fluid with negligible viscous and second order terms (this assumption is valid as long as frequency of sound source is below 1 MHz (Ref. 13)) has two alternative forms, named as enthalpy form and internal energy form[19]

$$\rho\frac{\partial h}{\partial t}=\frac{\partial p}{\partial t}+k\nabla^2 T, \tag{1}$$

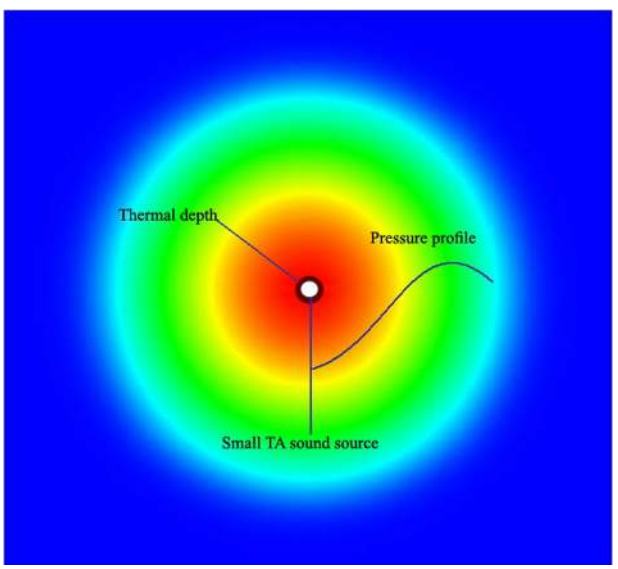

FIG. 1. Spherical control volume around a small TA source which has radius equals to one wave length. Thermal waves penetrate into a small distances while pressure waves propagate to infinite medium and are much bigger than thermal depths in frequency below 1 MHz (Ref. 13). Pressure profile after one periodic cycle around the small source is shown.

$$\rho\frac{\partial e}{\partial t}=k\nabla^2 T, \tag{2}$$

where k, ρ, h, and e are conductivity, density, enthalpy, and internal energy of fluid, respectively. Assuming that the surrounding fluid is an ideal gas and integrating two alternative forms of energy, Eqs. (1) and (2) inside control volume of Fig. 1 yields

$$C_p\int_{r_0}^{\lambda_p}\rho\frac{\partial T}{\partial t}(4\pi r^2)dr=\int_{r_0}^{\lambda_p}\frac{\partial p}{\partial t}(4\pi r^2)dr+\dot{Q}_{fluid-transient}, \tag{3}$$

$$C_v\int_{r_0}^{\lambda_p}\rho\frac{\partial T}{\partial t}(4\pi r^2)dr=\dot{Q}_{fluid-transient}, \tag{4}$$

where $r_0\cong 0$, λ_p, and $\dot{Q}_{fluid-transient}$ are sound source radius, pressure wave length, and instantaneous periodic heat delivered to the fluid at the surface of the source due to conduction, respectively.

Pressure after on cycle inside control volume radiated from a point source has the following form[20] as shown in Fig. 1:

$$p(r)=\frac{p_{\lambda_p}\times\lambda_p}{r}\times(-\sin(k_0 r)), \tag{5}$$

where p_{λ_p} is pressure amplitude at $r=\lambda_p$ and $k_0=\frac{2\pi}{\lambda_p}$.

Combining these three above equations, results in (See Appendix)

$$p_{rms}=\frac{f}{2\sqrt{2}C_p T_0 r}\times\dot{Q}_{fluid}. \tag{6}$$

Equation (6) gives contributions inherent to thermo acoustic phenomenon. In case of negligible heat capacity of TA source, heat delivered to the fluid equals the electrical input energy and Eq. (6) would be exactly the same as a limiting case of other theories developed by different manners.[3,6,11] However, in general case, heat capacity of TA source plays a key role in delivering heat to the medium and must be considered in the analysis. Although Eq. (6) is derived for the small heat sources, it can also be used to predict pressure generation of finite size sources like CNT sheets in far field where dimensions of the source do not affect the pressure field.

Now, to calculate the energy delivered to the fluid $\dot{Q}_{fluid}$ in Eq. (6) consider a free standing TA source, like CNTs sheet. Writing energy balance for TA sound source as shown in Fig. 2, we have

$$P_e=\dot{Q}_s+\dot{Q}_{fluid}, \tag{7}$$

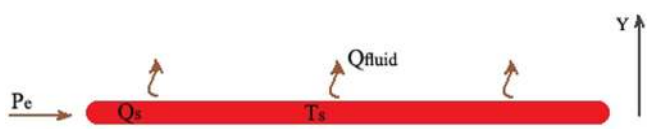

FIG. 2. Schematic of heat balance in a TA sound source. Part of input energy is consumed in TA sound source and the rest is conducted to the surrounding medium.

where $\dot{P}_e$ and $\dot{Q}_s$ are electrical power input and heat consumed in sound source, respectively.

Equation (7) states that part of the input energy is consumed by the sound source as $\dot{Q}_s$ and the rest is conducted to the adjacent fluid as $\dot{Q}_{fluid}$ which contribute in thermo-acoustic effect.

In case of thin sound sources like CNT sheet, temperature across the source is assumed to be uniform and one directional (this assumption is true for sources like CNTs sheet which CNTs are uniformly distributed inside the sheet.). Internal form of energy Eq. (2) in one dimensional form is

$$\rho C_v \frac{\partial T}{\partial t} = k \frac{\partial^2 T}{\partial y^2}, \tag{8}$$

$$T = T_s = T_0 \sin(\omega t) \quad \text{at } y = 0 \text{ (B.C)}, \tag{9}$$

where T_s and T_0 are temperature and amplitude of temperature in TA sound source. Alternative input energy leads to a periodic temperature variation of source as a boundary condition. Solution of Eq. (8) is[21]

$$T = T_0 \exp(-k_1 y) \times \sin(\omega t - k_1 y), \tag{10}$$

where $k_1 = \sqrt{\frac{\rho C_v \omega}{2k}} = \sqrt{\frac{\pi f}{\alpha_v}}$ and $\alpha_v = \frac{k}{\rho C_v}$. Now, having temperature distribution in fluid we can calculate $\dot{Q}_{fluid}$ and $\dot{Q}_s$. By substituting them in Eq. (7), energy reached to the fluid is calculated (See Appendix)

$$\dot{Q}_{fluid\_aerogel} = \frac{1}{1 + \frac{HCPUA}{\rho C_{v_{fluid}} \left(\sqrt{\frac{2\alpha_v}{\pi f}} + d_{sf} \right)}} . P_e. \tag{11}$$

In the above equation, $\dot{Q}_{fluid\_aerogel}$ is for general case where sound source has thickness of d_{sf} with aerogel nature like CNTs sheet sources. For non-aerogel sound sources d_{sf} vanishes in above equation. Note the above equation is expressed as thermal diffusivity and specific heat capacity at constant volume for the medium gas. Equation (11) measures ability of TA source in delivering heat to the surrounding fluid.

Now substituting value of $\dot{Q}_{fluid}$ from Eq. (11) in Eq. (6), pressure value can be expressed as

$$p_{rms} = \frac{1}{1 + \frac{HCPUA}{\rho C_{v_{fluid}} \left(\sqrt{\frac{2\alpha_v}{\pi f}} + d_{sf} \right)}} \cdot \left[\frac{f}{2\sqrt{2} C_p T_0 r} . P_e \right]. \tag{12}$$

Equation (12) explicitly separates the contributions inherent to thermo-acoustics (terms inside brackets) and those specific to the sound source (first term in above equation) where combining these two effects together gives sound generation of TA sources.

III. NUMERICAL

Consider a TA sound source is producing sound in open space. Figure 3 shows schematic of propagation of sound from this sound source in one eighth of space. Governing equations for thermo-acoustic effect, in addition of energy equation (1) and equation of state $(P = \rho RT)$, are continuity and momentum equations for compressible, unsteady moving fluid with negligible viscous and second order terms[19]

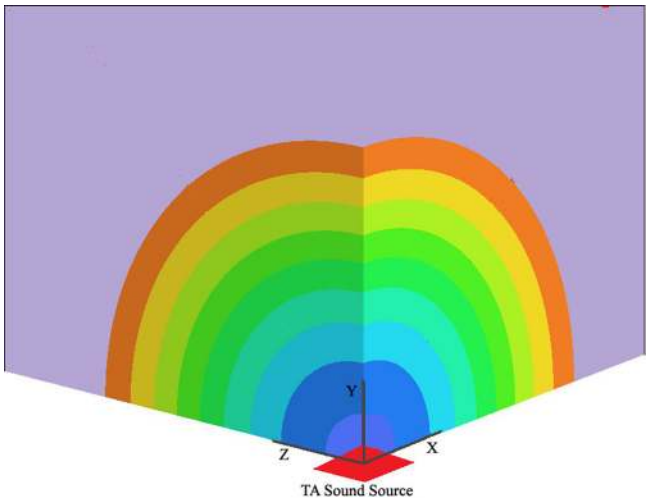

FIG. 3. Schematic of propagation of waves from a TA sound source in eighth of space. Sound generation is symmetric respected to the *x*-*y*, *x*-*z*, and *y*-*z* planes.

$$\frac{D\rho}{Dt} + \rho \nabla . V = 0, \tag{13}$$

$$\rho \frac{DV}{Dt} = -\nabla P. \tag{14}$$

With the following boundary conditions:

$$q_{gen} = \dot{Q}_{fluid\_aerogel} \quad \text{at } y = 0, \tag{15}$$

$$p = p_{sur} = cte \text{ at } r \to \infty. \tag{16}$$

Note that taking advantages of Eq. (11), we could avoid modeling of carbon nanotube sheet which is composed of many Multi Wall Carbon Nanotubes (MWCNTs). Microscopic picture of these webs shows that these sheets are approximately 90% porous, that is, only about 10% of the volume of this aerogel sheet is occupied by CNTs and the CNT sheet is impregnated with surrounding fluid. So we can assume periodic heat is generated within a rectangular cubic of fluid with height of 20 μm. The only effect of CNTs is that they consume a portion of input electrical energy because of their heat capacity which Eq. (11) accounts for this energy wasted at TA source. Equation (15) shows this heat generation as a boundary condition at y = 0.

Using second order finite difference method for time and spatial derivatives, governing Eqs. (1), (13), and (14) are solved in a cubic domain in which the pressure waves are propagated. Because of rectangular shape Of TA sound source in this problem, here instead of using sphere domain around TA sound source, a cubic domain is used to avoid high skewness of meshes. For a rectangular cubic TA source inserted in open space (Fig. 3), the domain of solution is symmetric respect to the *x*-*y*, *x*-*z*, and *y*-*z* planes. Consequently, three symmetry boundary conditions are used

which lead to a domain size of one eighth of the main domain size. To satisfy boundary condition stated in Eq. (16), a constant pressure (ambient pressure) is considered on outer surfaces of the domain. Note that here dimensions of solution are big enough where waves do not reach outer surfaces during solution. In vicinity of TA source where thermal waves are generated, size of grids is $\lambda_T/32$ and in the rest of the domain where pressure waves are propagated, sizes of grid is $\lambda_p/16$ where λ_T and λ_p are thermal and pressure wave length, respectively.[21]

IV. EXPERIMENT

In order to verify our numerical and theoretical solution, here sound generation of CNT based sources are measured experimentally. Three different CNT sound sources with surface area of 3×3, 5×5, and $10 \times 10\,\text{cm}^2$ are used for this study. Figures 4(a) and 4(b) show two of these CNT projectors. An AC voltage is applied to the sound source by signal generator (Bruel & Kjar) and then sound pressure level is measured by an accurate Sound Level Meter (SLM) (Bruel & Kjar, type 2250). Experiment was implemented in a silence room to minimize the environment noise (Fig. 4(c)). To study pressure field, we measured sound pressure at difference distances. For this purpose, SLM was mounted on a scaled rod which provides accurate one directional movement for SLM (Fig. 4(d)).

V. RESULTS

Figure 5 shows theoretical, numerical, and experimental results for two different sizes of CNT sound source as function of distance. For larger area of CNT sheets, there is a large discrepancy between theoretical and experimental data in near field, which is attributed to the 3 dimensional effects of pressure waves. However, as distance from the source increases, theoretical data approach to its true value measured by the experiment (Figs. 5(a) and 5(b)). Rayleigh distance is an approximate criterion to predict distance through which wave interference takes place[22]

$$R_0 = \frac{A}{\lambda_p}, \tag{17}$$

where A is surface area of source and λ_p is pressure wavelength. For TA source surface of $100\,\text{cm}^2$ at frequency of 5 and 20 KHz in the air, Rayleigh distance is about 14.5 and 57 cm. That indicates if measuring distance is far enough, larger than Rayleigh distance, Eq. (12) can be used with confidence to predict sound generation of TA sound sources. In case of smaller sound source at lower frequencies, where interference of pressure waves occurs at nearer distances, theory is able to accurately predict sound intensity in more distances (Fig. 5(c)).

In general, for small TA source, 1D model is applicable for pressure calculation in more distances compared to the larger sources and if measuring point is far enough from the source, 1D model agrees well for all sources.

To truly calculate ability of TA sound sources as a function of frequency, one must make sure that measuring point is in far field region for all frequencies. For a sound source of $50 \times 50\,\text{mm}^2$ at measuring point of $r = 0.5\,\text{m}$, frequency at which interference effect happens is around 68 KHz, examined by Suzuki *et al.*[10] So it is expected at this frequency, sound intensity deviate from its linear dependence on frequency.

Figure 5 also shows numerical results, which take all 3 dimensional effects into account, are more consistent with experimental data both in near and far fields. This consistency ensures only thermo acoustic effect, without any possible vibration of CNTs sheet, is responsible for the sound generation in a TA source.

To study effect of area surface of projectors, we used three CNTs sound source with surface area of $9\,\text{cm}^2$, $25\,\text{cm}^2$, and $100\,\text{cm}^2$. Figure 6 shows results of these three projectors at two frequencies for the same input power. In spite of

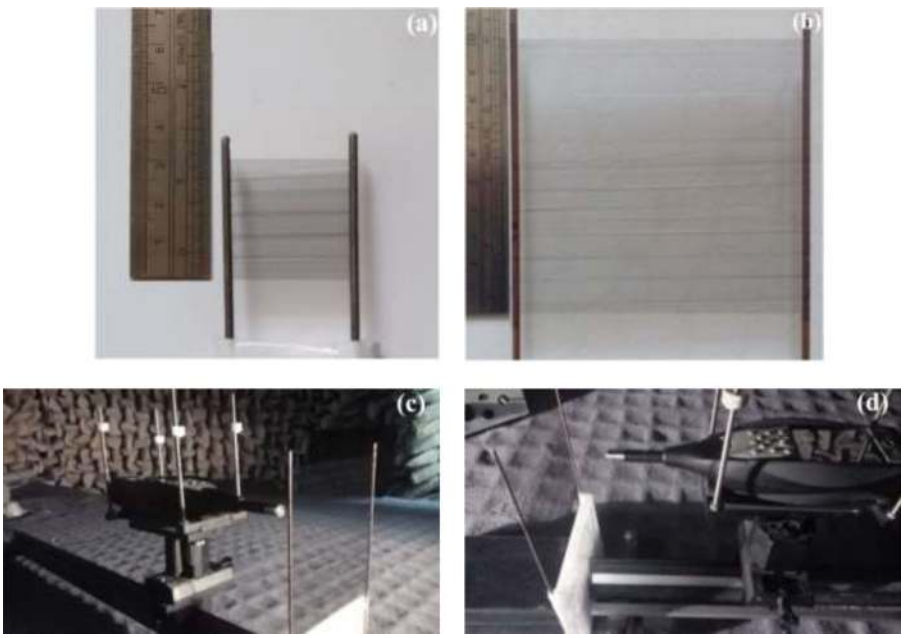

FIG. 4. CNT projectors and experimental setup. (a) $3 \times 3\,\text{cm}^2$ (b) $10 \times 10\,\text{cm}^2$. (c) Silence room with $10 \times 10\,\text{cm}^2$ CNT projectors and a SLM to measure sound intensity. (d) SLM is mounted on a scaled rod with freedom of sliding in one dimensional.

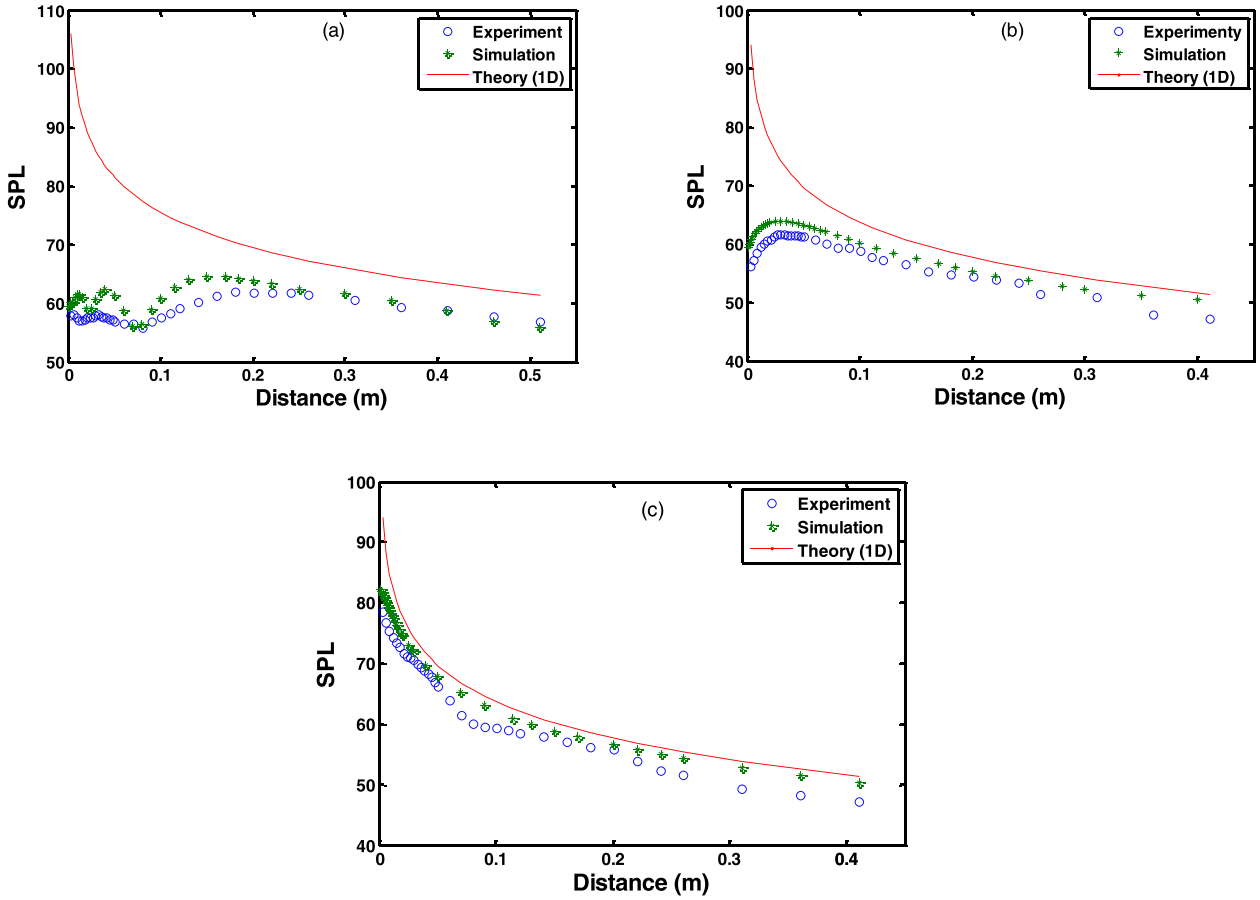

FIG. 5. Theoretical, simulation and experimental results of TA projectors for. (a) Surface area of 100 cm^2 at frequency of 20 KHz. (b) Surface area of 100 cm^2 at frequency of 5 KHz. (c) Surface area of 9 cm^2 at frequency of 5 KHz. Power input for (a), (b), and (c) is 0.6, 0.6, and 0.5 W, respectively.

different pressure amplitude in the near field, sound pressure in the far field for these three sources reach to the same amount. This means that using large surface area projectors does not affect pressure amplitude in the far field. However, maximum input power applied per unit area of these sound projectors (about 50 kw/m^2 for one layer CNTs sheet[3]) is a barrier to reach small size TA sources especially at high-powered applications. Figure 7 shows contour of pressure at frequency of 20 KHz for these three different sources. At the same frequency and input power, maximum of SPL generated by these TA sources occur at different distances with different magnitudes. In case of CNTs sheet, this is of special importance because these sound sources are flexible and could take many shapes and forms. At higher frequencies, this could help focusing of pressure field at a specified location to reach higher sound intensity at desired point which could be applicable in some medical applications like lithotripsy for breaking of kidney stones.

Figure 8(a) shows portion of energy transferred to the air by aerogel TA sources (with typical thickness of 20 μm)

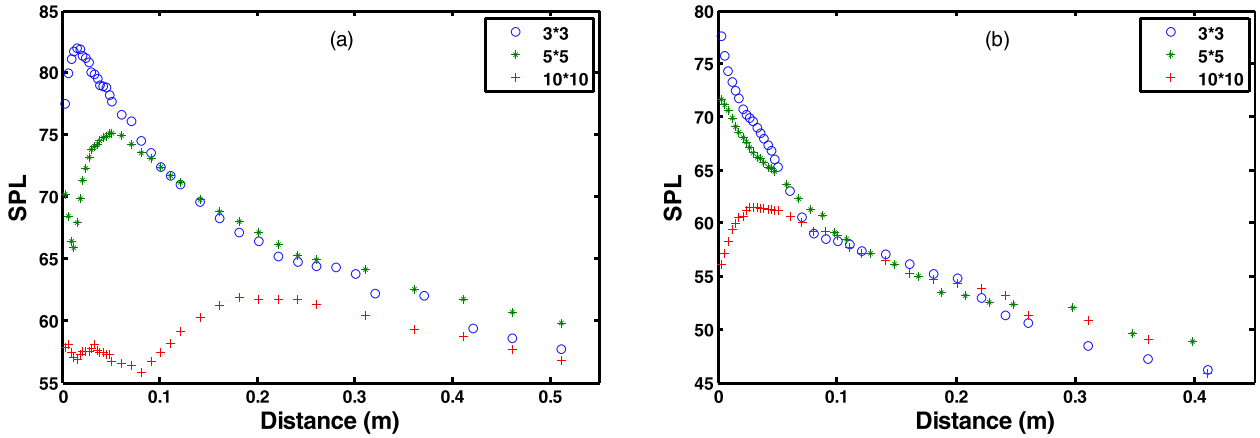

FIG. 6. Sound pressure of different sizes of CNT sheet. (a) At frequency of 20 KHz. (b) At frequency of 5 KHz. Input power for all samples is 0.6 W.

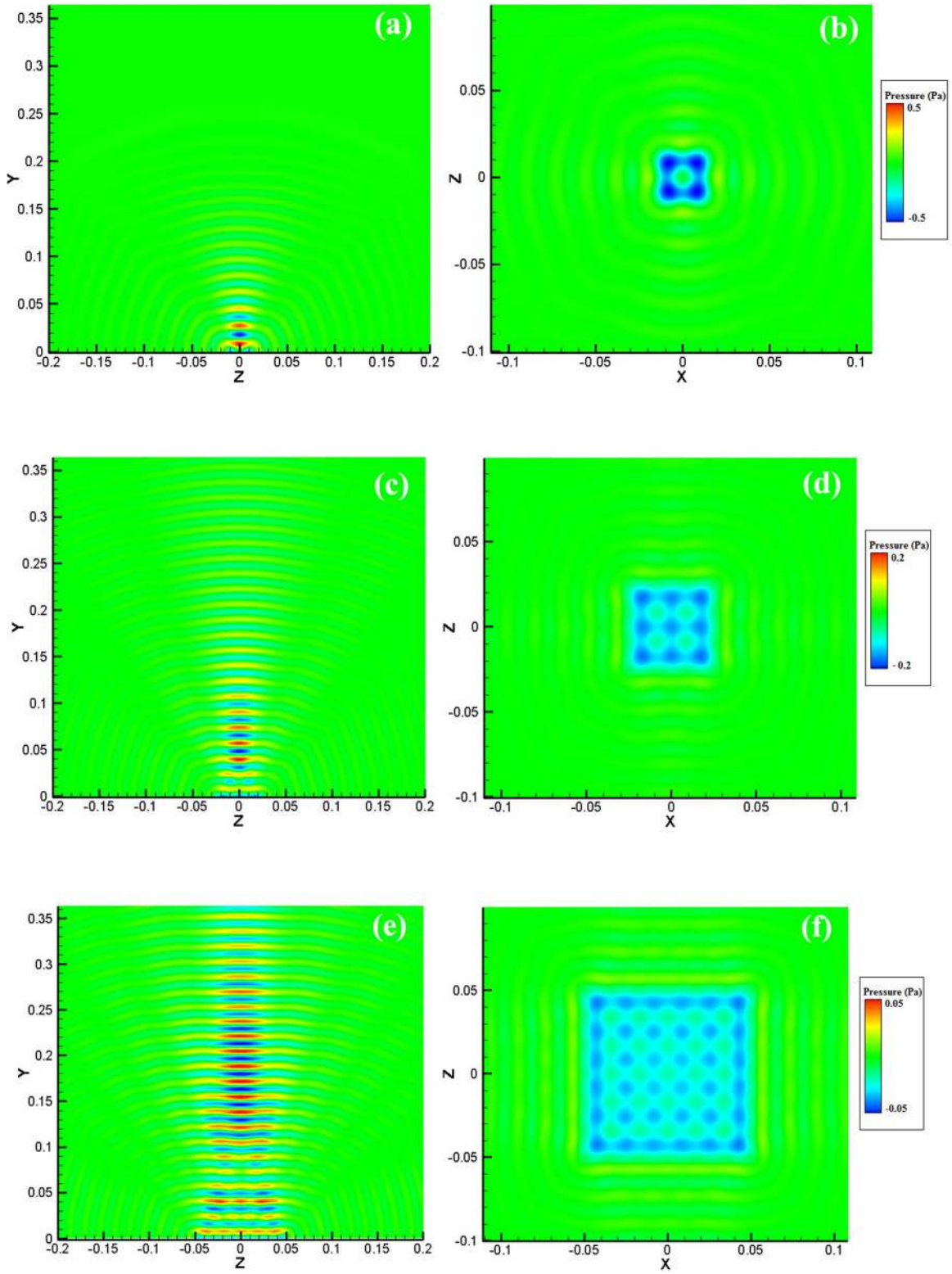

FIG. 7. Near field sound generation of three different sizes of CNT sheets at the same frequency of 20 KHz. Pressure contours for three different area surfaces for $3 \times 3\,cm^2$ (a, b), $5 \times 5\,cm^2$ (c, d), $10 \times 10\,cm^2$ (e, f). The left ones are at $x = 0$ and the right ones are at $y = 0$ plane.

as a function of HCPUA for different frequencies, derived from Eq. (11). For sound projectors with HCPUA larger than $10\,J/m^2k$, almost all energy is consumed in projector itself and no energy is conducted to the medium. As a consequence, these sources are impractical for TA applications. As the HCPUA of projector decreases, more and more energy is delivered to the fluid until almost all energy is conducted to the air. CNT sound source have HCPUA around[3] $7.7 \times 10^{-3}\,J/m^2k$ and it is nearly perfect material when used in TA because it delivers more than 75% of energy to the medium for frequencies up to 1 MHz. Part of the this faithful behavior of CNT sheet is related to the aerogel

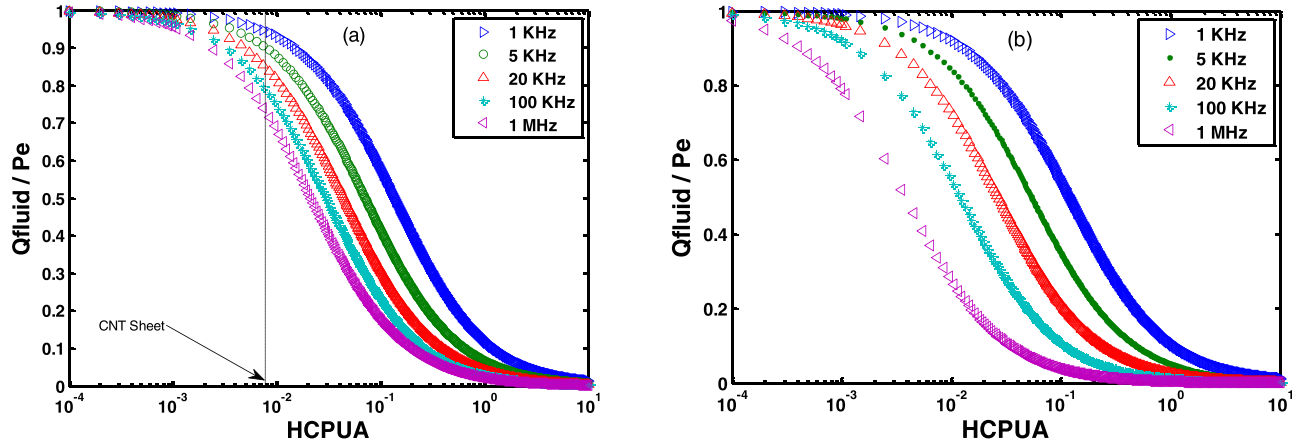

FIG. 8. Portion of input energy delivered to the medium fluid by free standing TA sources for. (a) Aerogel TA sound sources (thickness of 20 μm). CNT based projectors deliver more than 75% of input energy to the surrounding medium in frequencies below 1 MHz. (b) Non-aerogel TA sound sources. At a given HCPUA, ability of non-aerogel TA sources degrades more rapidly at higher frequencies compared to the aerogel sources.

nature of these webs. In these sound sources, medium fluid could permeate into empty space inside CNT sheet. As a consequence, heat transferred to the medium fluid is a volumetric phenomenon that enhances thermo acoustic effect. This is especially important at higher frequencies where thermal depth is smaller. In other non-aerogel sound sources, heat conduction to the medium only occurs in the surfaces of source. Figure 8(b) shows portion of energy reached to the medium fluid for these sound sources at free standing state. It can be seen if the HCPUA of source get bigger, their performance at higher frequencies degrades and sound generation ability of TA sources decreases more rapidly compared to the aerogel TA sources at the same magnitude of HCPUA. Therefore, one way for efficient behavior of TA sources at higher frequencies is to make sound sources with aerogel nature. That is why far field frequency response of CNT sound sources shows no obvious decrease, up to frequency of 100 KHz.[11]

Upper limit of frequency response of CNT projector is still unknown and to determine their ability for sound generation at frequencies of MHz domains, attenuation of sound due to viscosity effects should also be considered.[18]

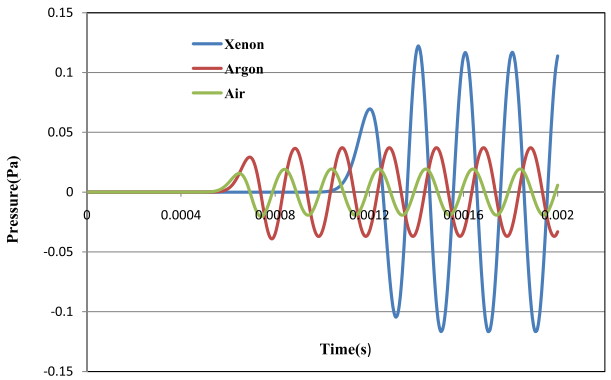

FIG. 9. Snapshot of pressure variation at location of (0, 0.2, 0) for three different gases. Because sound speed in air and Argon is more than sound speed of Xenon, pressure pulses in these gases arrive much sooner to the measuring point.

However, energy analysis of these sources indicates their faithful behavior in delivering energy to medium gas in these frequencies.

Equation (12) indicates that in addition of dependence of pressure to the inverse heat capacity of surrounding gas, pressure is also dependent on ability of the gas in receiving energy from sound source. This ability relates to the thermal properties of fluid. Here, we also solved governing 3-D equations for Xenon and Argon numerically. Figure 9 shows a snapshot of simulation result at $t = 0.002$ s for these two gases and the air at distance of 20 cm far from origin with coordinates of (0, 0.2, 0). Note that because sound speed differs for different gases, it took about twice time for Xenon (compared to the air) until pressure wave reaches to the measuring point from its generation location. That is in good agreement with sound speed in air and Xenon which is 345 and 169 m/s, respectively. Table I compares results of pressure ratio predicted by Eq. (12), FD simulation, and experimental data.[13]

As a final point, here temperature field around TA sound source with surface area of 25 cm^2 at 5 KHz are depicted in Fig. 10. It can be seen that temperature wave permeate into small distance through medium and by rapid variation of these temperatures, pressure waves are generated and propagated in medium. In calculation of portion of energy delivered to the fluid, we assumed temperature distribution is uniform across CNT sheet and its variation is just in one directional. Figure 10 which is a three dimensional solution of the governing equations confirms the fact that temperature variation, with acceptable approximation, could be considered one-directional.

TABLE I. Results of pressure ratio for Argon and Xenon compared to the air.

	$\frac{C_{p-air}}{C_{gas}}$	$\frac{P_{gas}}{P_{air}}$ (Eq. (12))	$\frac{P_{gas}}{P_{air}}(FD)$	$\frac{P_{gas}}{P_{air}}$ (Exp[13])
Argon	1.92	1.81	1.76	1.50
Xenon	6.32	5.54	5.41	5.21

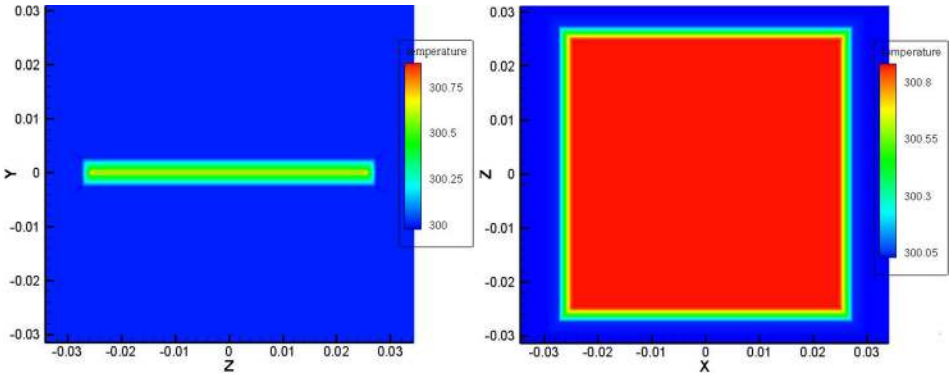

FIG. 10. Snapshot of temperature contours around a TA source with dimensions of $5 \times 5\,\mathrm{cm}^2$ at frequency of 5 KHz. The left one is at $x = 0$ plane which shows temperature variation approximately take place in one direction. The right one is at $y = 0$ plane indicating uniform distribution of temperature in most area of TA surface.

VI. CONCLUSION

We derived a formula for sound generation of small TA sound sources using two alternative forms of energy in terms of energy conducted to the fluid. Using energy equation for source and medium fluid, the energy transferred to the fluid by finite free standing TA source is calculated, which lead to a model for prediction of sound generation of TA projectors which could accurately predict sound generation in far field. To study pressure in near field, full 3-D governing equations are solved by a numerical method which is able to account for all three dimensional thermal and pressure wave interactions near sound source. Although near field pressure is highly affected by sizes of TA projectors, far field pressure is independent of sound source dimensions.

Analyzing the ability of TA sound sources in faithfully delivering input energy to the medium fluid shows CNT based projectors are almost optimum material for TA sound generation in ultra sound region, thanks to their aerogel nature in addition of their ultra-small HCPUA.

Temperature contour around TA source shows temperature variation is approximately one dimensional.

Ability of CNT based projectors in producing sound in ultra sound range, together with their flexibility to take many shapes and forms, may be beneficial in manufacturing devices that could be useful in industrial and medical applications.

ACKNOWLEDGMENTS

We thank Dr. Ahmad Amjadi and Nima Jafari (Physics Department of Sharif University of Technology) for providing experimental setup and their helpful advice for conducting experiments. Solution steps to derive sound generation of small TA source are provided as below:

APPENDIX: DETERMINATION OF SOUND PRESSURE AND HEAT DELIVERED TO MEDIUM

Calculation of Eq. (6):

Calculating $\int_{r_0}^{\lambda_p} \rho \frac{\partial T}{\partial t}(4\pi r^2)dr$ from Eq. (4) and substituting it in Eq. (3) yields

$$(\gamma - 1)\dot{Q}_{fluid\_transient} = \int_{r_0}^{\lambda_p} \frac{\partial p}{\partial t}(4\pi r^2)dr,$$

where $\gamma = \frac{C_p}{C_v}$. Integrating above equation in one period of input energy yields

$$(\gamma - 1)\dot{Q}_{fluid} \times 1/f = \int_{r_0 \cong 0}^{\lambda_p} p(r) \times (4\pi r^2)dr,$$

where $\dot{Q}_{fluid}$ and f are mean value of heat generation and frequency, respectively. The right side of this equation is equal to mean heat generation in one periodic cycle.

Now substituting magnitude $p(r)$ from Eq. (5) in above equation yields

$$(\gamma - 1)\dot{Q}_{fluid} \times \frac{1}{f} = 4\pi \times p_{\lambda_p} \times \lambda_p \int_0^{\lambda_p} -r \times \sin(k_0 r)dr$$
$$= 4\pi \times p_{\lambda_p} \times \lambda_p \times \frac{{\lambda_p}^2}{2\pi}.$$

Pressure value at $r = \lambda_p$ is calculated as

$$p_{\lambda_p} = \frac{(\gamma - 1)}{2\lambda_p^3} \times \frac{\dot{Q}_{fluid}}{f}.$$

Multiplying this equation by $\frac{\lambda_p}{r}$ and considering $\lambda_p = \frac{v_0}{f}$ yields

$$p = \frac{(\gamma - 1)}{2r \times \lambda_p^2} \times \frac{\dot{Q}_{fluid}}{f} = \frac{(\gamma - 1) \times f}{2r \times v_0^2} \times \dot{Q}_{fluid}.$$

For ideal gases, $v_0^2 = \gamma R T_0$ and $R = C_p - C_v$. Substituting these terms in above equation results in Eq. (6).

Calculation of Eq. (11):

To derive energy transferred to the fluid as in Eq. (7), we can write

$$\dot{Q}_{fluid\_transient} = 2\int \rho A C_{v_{fluid}} T_0 \omega . \exp(-k_1 x) \times \sin(\omega t - k_1 x)dx$$
$$= 2\rho A C_{v_{fluid}} T_0 \omega \int \exp(-k_1 x) \times \sin(\omega t - k_1 x)dx$$
$$= 2\rho A C_{v_{fluid}} T_0 \omega \times \frac{\exp(-k_1 x)}{\sqrt{2}k_1}$$
$$\times \sin\left(\omega t - k_1 x - \frac{\pi}{4}\right)\Bigg\{ \begin{matrix} \infty \\ 0 \end{matrix}$$
$$= 2\rho A C_{v_{fluid}} T_0 \omega \times \frac{1}{\sqrt{2}k_1} \sin\left(\omega t - \frac{\pi}{4}\right),$$

considering $k_1 = \sqrt{\frac{\pi f}{\alpha_v}}$, effective value of $\dot{Q}_{fluid\_transient}$ is calculated

$$\dot{Q}_{fluid} = \rho A C_{v_{fluid}} T_0 \omega \times \sqrt{\frac{\alpha_v}{\pi f}}.$$

In case of aerogel sound sources like CNTs sheet, the fluid inside the aerogel sheet is also heated with uniform temperature variation equal to temperature variation of source and this heat must be added to the $\dot{Q}_{fluid}$. Effective value of this heat is

$$\dot{Q}_{inside} = \rho A C_{v_{fluid}} T_0 \omega \frac{d_{sf}}{\sqrt{2}},$$

where d_{sf} is thickness of aerogel sound source. For one layer CNTs sheet, its value is typically about 20 μm and it vanishes for other sources without having porous property. Adding to above equations gives energy delivered to the fluid by an aerogel TA sound source

$$\begin{aligned}\dot{Q}_{fluid\_aerogel} &= \rho A C_{v_{fluid}} T_0 \omega \times \sqrt{\frac{\alpha_v}{\pi f}} + \rho A C_{v_{fluid}} T_0 \omega \frac{d_{sf}}{\sqrt{2}} \\ &= \rho A C_{v_{fluid}} T_0 \omega \left(\sqrt{\frac{\alpha_v}{\pi f}} + \frac{d_{sf}}{\sqrt{2}} \right).\end{aligned}$$

Portion of energy consumed in sound sources is

$$\dot{Q}_s = \rho_s A C_s T_0 \omega \frac{d_{sf}}{\sqrt{2}}.$$

Now having $\dot{Q}_{fluid\_aerogel}$ and $\dot{Q}_s$ and substituting them into Eq. (7), $\dot{Q}_{fluid\_aerogel}$ is calculated

$$\begin{aligned}\dot{Q}_{fluid\_aerogel} &= \frac{\dot{Q}_{fluid\_aerogel}}{\dot{Q}_s + \dot{Q}_{fluid\_aerogel}} . P_e \\ &= \frac{\rho A C_{v_{fluid}} T_0 \omega \left(\sqrt{\frac{\alpha_v}{\pi f}} + \frac{d_{sf}}{\sqrt{2}} \right)}{\rho A C_{v_{fluid}} T_0 \omega \left(\sqrt{\frac{\alpha_v}{\pi f}} + \frac{d_{sf}}{\sqrt{2}} \right) + \rho_s A C_s T_0 \omega \frac{d_{sf}}{\sqrt{2}}} . P_e\end{aligned}$$

$$\dot{Q}_{fluid\_aerogel} = \frac{1}{1 + \frac{\rho_s C_s d_{sf}}{\rho C_{v_{fluid}} \left(\sqrt{\frac{2\alpha_v}{\pi f}} + d_{sf} \right)}} . P_e.$$

[1] H. D. Arnold and I. B. Crandall, "The thermophone as a precision source of sound," Phys. Rev. **10**, 22–38 (1917).
[2] X. Zhang *et al.*, "Spinning and processing continuous yarns from 4-inch wafer scale super-aligned carbon nanotube arrays," Adv. Mater. **18**, 1505–1510 (2006).
[3] L. Xiao *et al.*, "Flexible, stretchable, transparent carbon nanotube thin film loudspeakers," Nano Lett. **8**, 4539–4545 (2008).
[4] A. E. Aliev, M. D. Lima, S. Fang, and R. H. Baughman, "Underwater sound generation using carbon nanotube projectors," Nano Lett. **10**, 2374–2380 (2010).
[5] A. O. Niskanen *et al.*, "Suspended metal wire array as a thermoacoustic sound source," Appl. Phys. Lett. **95**, 163102 (2009).
[6] V. Vesterinen, A. O. Niskanen, J. Hassel, and P. Helisto, "Fundamental efficiency of nanothermophones: Modeling and experiments," Nano Lett. **10**, 5020–5024 (2010).
[7] H. Tian *et al.*, "Transparent, flexible, ultrathin sound source devices using indium tin oxide films," Appl. Phys. Lett. **99**, 043503 (2011).
[8] H. Tian *et al.*, "Graphene-on-paper sound source devices," ACS Nano **5**, 4878–4885 (2011).
[9] G. Ghitnis *et al.*, "A thermophone on porous polymeric substrate," Appl. Phys. Lett. **101**, 021911 (2012).
[10] K. Suzuki *et al.*, "Study of carbon-nanotube web thermoacoustic loudspeakers," Jpn. J. Appl. Phys. Part 1 **50**, 01BJ10 (2011).
[11] L. Xiao *et al.*, "High frequency response of carbon nanotube thin film speaker in gases," J. Appl. Phys. **110**, 084311 (2011).
[12] A. R. Barnard *et al.*, "Feasibility of a high-powered carbon nanotube thin-film loudspeaker," J. Acoust. Soc. Am. **134**, EL276–EL281 (2013).
[13] A. E. Aliev, Y. N. Gartstein, and R. H. Baughman, "Increasing the efficiency of thermo-acoustic carbon nanotube sound projectors," Nanotechnology **24**, 235501 (2013).
[14] H. Hu, Y. Wang, and Z. Wang, "Wideband flat frequency response of thermo-acoustic emission," J. Phys. D: Appl. Phys. **45**, 345401 (2012).
[15] H. Hu, T. Zhu, and J. Xu, "Model for thermoacoustic emission from solids," Appl. Phys. Lett. **96**, 214101 (2010).
[16] H. Hu *et al.*, "Analysis of spherical thermo-acoustic radiation in gas," AIP Adv. **2**, 032106 (2012).
[17] H. Hu, Y. Wang, and Z. Wang, "Solution for acoustic field of thermo-acoustic emission from arbitrary source," AIP Adv. **4**, 107114 (2014).
[18] M. Daschewski *et al.*, "Physics of thermo-acoustic sound generation," J. Appl. Phys. **114**, 114903 (2013).
[19] J. D. Anderson, *Modern Compressible Flow with Historical Perspective* (McGraw-Hill, 2003).
[20] P. M. Morse, *Theoretical Acoustics* (Princeton University Press, 1986).
[21] M. N. Ozisik, *Heat Conduction* (John Wiley & Sons, 1993).
[22] D. Ensminger and L. J. Bond, *Ultrasonics: Fundamentals, Technologies, and Applications* (CRC Press, 2011).